

1
2
3
4
5
6
7
8
9
10
11
12
13
14
15
16
17
18
19

Nonlinear and Synergistic Effects of ULF Pc5, VLF Chorus, and EMIC Waves on Relativistic Electron Flux at Geosynchronous Orbit

Laura E. Simms¹, Mark J. Engebretson¹, Mark A. Clilverd², Craig J. Rodger³, and Geoffrey D. Reeves⁴

¹ Augsburg University, Minneapolis, MN, USA

² British Antarctic Survey (NERC), Cambridge, UK

³ University of Otago, Dunedin, New Zealand

⁴ Los Alamos National Laboratory, Los Alamos, New Mexico, USA

Key Points:

1. Regression analyses of relativistic electron flux (0.7-7.8 MeV) show both linear and non-linear response to wave activity.
2. High chorus intensity and mid-range ULF Pc5 power result in more electron acceleration than would be predicted by an additive model.
3. The negative effect of EMIC waves is greater if combined with either chorus or ULF Pc5 waves.

20 **Abstract**

21 Using data covering the years 2005-2009, we study the linear and nonlinear responses of \log_{10}
22 relativistic electron flux measured at geosynchronous orbit to ULF Pc5, VLF lower band chorus, and EMIC
23 waves. We use regression models incorporating a quadratic term and a synergistic interaction term.
24 Relativistic electron fluxes respond to ULF Pc5 and VLF chorus waves both linearly and nonlinearly. ULF
25 Pc5 waves contribute both to electron enhancement (at mid-range wave activity) and loss (at high levels
26 of wave activity). Nonlinear effects of VLF chorus are positive (i.e., cause acceleration), adding to the
27 positive linear effects. Synergistic interaction effects between high levels of VLF chorus and mid-range
28 values of ULF Pc5 waves result in more electron acceleration than would be predicted by a simpler
29 additive model. Similarly, the negative effect of EMIC waves (losses) is more influential than would be
30 predicted by a linear model when combined with either VLF chorus or ULF Pc5 waves. During disturbed
31 conditions (high K_p), geostationary electron flux responds more strongly to the same levels of ULF Pc5
32 and VLF chorus waves. This flux also responds more to ULF Pc5 and chorus waves during southward B_z
33 conditions. Unstandardized regression coefficients for models incorporating nonlinear and synergistic
34 effects of waves are presented for use in future modelling.

35

36 **1. Introduction**

37 At geosynchronous orbit, the level of relativistic electron flux is in part controlled by wave-particle
38 interactions. Flux enhancement follows both enhanced ULF Pc5 wave activity (ultralow frequency; 2-7
39 mHz) (Borovsky & Denton, 2014; Degtyarev et al., 2009; Lam, 2017; Mathie & Mann, 2000; Mann et al.,
40 2004; O'Brien et al., 2003; Rostoker et al., 1998; Simms et al., 2016; Su et al., 2015) and higher VLF lower
41 band chorus wave activity (very low frequency waves; 0.1 - 0.5 fce, the electron cyclotron frequency)
42 (Horne et al., 2005a; Iles et al., 2006; Meredith et al., 2002, 2003; Miyoshi et al., 2003; 2007; O'Brien et
43 al., 2003; Spasojevic & Inan, 2005; Thorne et al., 2013; Turner et al., 2013; 2014). EMIC (electromagnetic
44 ion cyclotron) waves contribute to electron loss through pitch angle scattering (Blum et al., 2015;
45 Clilverd et al., 2007; 2015; Engebretson et al., 2015; Gao et al., 2015; Li et al., 2014; Miyoshi et al., 2008;
46 Rodger et al., 2008; Summers & Thorne, 2003; Turner et al., 2014; Usanova et al., 2014).

47 Co-occurring ULF Pc5 waves and a VLF chorus wave proxy have been observed to increase relativistic
48 electron flux additively at lower L-shells ($L \sim 4.5$), although ULF Pc5 effects on flux dominated over the
49 VLF proxy at geosynchronous orbit (O'Brien et al., 2003). However, previously, we have found that VLF
50 chorus from L 4 (DEMETER satellite) correlates well with enhanced flux at geosynchronous orbit where it
51 acts additively in combination with ULF Pc5 effects to produce flux enhancements (Simms et al., 2018a,
52 in submitted (Paper 1)). There has also been speculation that any loss processes associated with VLF
53 and EMIC waves combine in their effects (Mourenas et al., 2016; Summers & Ma, 2000). Observational
54 evidence supports this theory of additive action by VLF and EMIC waves in their ability to scatter
55 ultrarelativistic electrons (Zhang et al., 2017).

56

57 However, the combined effect of several wave types on flux may not be simply a matter of adding their
58 influences together. They could act synergistically, with each factor having more or less influence at
59 varying levels of the other. This can be tested with an interaction term in multiple regression. By
60 multiplying the factors together and entering this new variable into the analysis, the hypothesis that
61 these factors do more than act additively can be tested.

62
63 In addition to these interactions (represented by a multiplicative factor in regression), wave effects may
64 not be linear over their whole range. Nonlinear effects can be explored with the addition of a squared
65 term, thereby creating a quadratic model.

66 Using regression techniques, we produce prediction models using wave parameters from observed data
67 inputs, incorporating both interaction terms and quadratic terms. In this study, we use autoregressive
68 models, to account for the high persistence of relativistic electron flux from day to day. We use data
69 only from the day previous to the flux measurement ("lag 1"), where wave effects are strongest, and
70 analyze only two wave types in each model so as to be able to present them graphically. In our previous
71 analyses (Simms et al., 2018a submitted (Paper 1)), predictor variables averaged over the day previous
72 to that on which flux was measured ("lag 1") correlated better with relativistic electron geostationary
73 flux; we therefore use lag 1 predictor data for our models here. As in our previous paper, we also add
74 an autoregressive (AR) term: the flux on lag 1. For example, the model incorporating ULF Pc5 and VLF
75 chorus would be represented as:

$$\begin{aligned} \text{Log Flux}_t = & b_0 + b_{AR} \times \text{Log Flux}_{t-1} + b_1 \times \text{ULF}_{t-1} + b_2 \times \text{ULF}^2_{t-1} + b_3 \times \text{Chorus}_{t-1} + b_4 \\ & \times \text{Chorus}^2_{t-1} + b_5 \times \text{ULF}_{t-1} \times \text{Chorus}_{t-1} \end{aligned} \quad (1)$$

76
77 Where b_0 is the intercept of the predicted regression line, b_{AR} the dependence of flux on its own value
78 the day before (the autoregressive term), b_1 and b_2 the slopes of the relationship between the linear and
79 quadratic (nonlinear component) ULF Pc5 terms with flux, b_3 and b_4 the parameters describing the
80 dependence on the linear and quadratic values of chorus, and b_5 the coefficient describing the
81 synergistic interaction effect of combined waves. This equation can be calculated by the ordinary least
82 squares method (Neter et al., 1985).

83 We analyze all available data with this model, then break the data into quiet times and disturbed times
84 for separate analyses. We also break the data into southward and northward Bz, based on the Bz daily
85 average.

86

87 **2. Data and Methods**

88 Over the years 2005-2009, we used daily averaged \log_{10} electron fluxes ($\log(\text{electrons}/(\text{cm}^2/\text{s}/\text{sr}/\text{keV}))$)
89 for relativistic electrons in four energy channels: 0.7-1.8, 1.8-3.5, 3.5-6.0, and 6.0-7.8 MeV. Flux data
90 comes from the Los Alamos National Laboratory (LANL) Energetic Spectrometer for Particles (ESP)
91 instruments located at geosynchronous orbit. ULF Pc5 was obtained from a ground-based ULF index
92 covering local times 0500 – 1500 in the Pc5 range (2-7 mHz) obtained from magnetometers stationed at
93 60-70° N CGM (Corrected GeoMagnetic) latitude (nT^2/Hz) (Kozyreva et al., 2007). VLF lower band
94 chorus (0.1 - 0.5 fce) daily-averaged intensity ($\log(\mu\text{V}^2/\text{m}^2/\text{Hz})$) is from the ICE (Instrument Champ
95 Electrique) on the Demeter satellite (Berthelier et al., 2006). We use L 4 (4.0-4.99), the highest L shell
96 for which there is good data coverage, averaged over the dayside passes of the satellite (LT 10:30). We
97 use pre-noon (dayside) chorus because it is found over a broader range of latitudes than pre-midnight
98 (nightside) chorus (Li et al., 2009; Thorne, 2010; Tsurutani & Smith, 1977).

99

100 Daily averages of IMF Bz and the Kp index are from the Omniweb database. Quiet times are defined as
101 the lowest 75 % of Kp measurements ($Kp < 2.3$, corresponding to the canonical Kp of <2+, 75% of the

102 data points or 1146 days). Disturbed time is the highest 25 % of Kp (Kp > 2.3 (>2+), 25% of the data
103 points or 387 days). The southward Bz category contains those days on which average Bz < -0.3 (lower
104 third, 511 days) while northward contains days where average Bz > 0.5 (upper third, 511 days).

105 EMIC wave power data is from the Halley, Antarctica BAS ground station located at L 4.6. We use the
106 number of hours per day during which there was high EMIC activity ($> 10^{-3} \text{ nT}^2 \text{ Hz}$) in the <1 Hz band.
107 Broadband activity was excluded.

108 For each of the four relativistic electron flux channels, using two wave types at a time, we perform
109 multiple regressions with a linear and a squared term for each predictor, along with an interaction term
110 derived from multiplying the two predictors together. The squared term fits a quadratic model to the
111 data for each variable, while the interaction term tests the ability of one variable to influence the action
112 of the other. As predictor data from one day previous ("lag 1") correlates better with relativistic
113 electron geostationary flux (Simms et al., 2018a submitted (Paper 1)), we use lag 1 predictor data in
114 these models. We also add an autoregressive (AR) term: lag 1 flux. This reduces the autocorrelation in
115 the time series analysis so that the assumptions of regression analysis are not violated, as well as
116 removing the effect of flux persistence so we can clearly see the effects of waves. We use
117 unstandardized regression coefficients to produce the figures in order to show the influence of each
118 variable on its own measurement scale. Graphs of the fitted regression equations (e.g., equation 1)
119 derived from observed data are shown in the figures. Note that the z-axis (\log_{10} flux) varies between
120 each panel. Putting them on the same scale would have obscured any patterns due to the wide
121 variation in flux associated with each variable at each energy level. However, the color scale (showing
122 the \log_{10} flux levels) is the same across all panels and figures.

123 Statistical analyses were performed in IBM SPSS Statistics, IDL, and MATLAB. Statistically significant
124 regression coefficients (p-value < .05 as reported in the results) mean that we have reasonable
125 confidence that there is an actual association between the variables. The p-value gives the probability
126 that the null hypothesis is true (i.e., no association) given the distribution of the data. Thus, a low p-
127 value gives us reason to reject the null hypothesis and accept that there is an association between
128 variables. Non-significant results (p-value > 0.05) mean we do not have enough evidence to reject this
129 correlation between parameters (Neter et al., 1985). The setting of 0.05 as the arbitrary level for
130 statistical significance is well established (e.g., Cowles and Davis, 1982 provide a historical perspective).

131
132

133 **3. Results**

134 Figure 1 shows the regression analyses for all available data. Four separate energy channels are shown
135 on each row, with row A depicting the response of the LANL \log_{10} relativistic electron fluxes to variations
136 in VLF chorus and ULF Pc5 wave intensity. In order to reduce congestion in the plots the units of each
137 parameter are not added to the plot labels (but are defined in Section 2 above). Row B compares the
138 influence of EMIC and ULF Pc5 waves on the \log_{10} electron fluxes, while row C compares EMIC and VLF
139 chorus waves.

140 The influence of ULF Pc5 does not follow a linear trend over its whole observed range (Figure 1 A and B,
141 Table 1 and 2). The peak influence occurs at mid-range powers ($\sim 60 \text{ nT}^2/\text{Hz}$; letter a of Figure 1A).
142 These trends are also visible in 1B but are not labeled). Above this mid-range, the influence of ULF Pc5

143 decreases, with the lowest influence at the highest levels of the index (b). This is described by the
144 negative quadratic term and is strongest in the lowest three energy channels (Table 1, the coefficients of
145 the ULF Pc5² term). However, because the positive linear effect leading to increased flux is smaller
146 above 6.0 MeV, the major factor at this highest energy is the negative quadratic effect, resulting in a low
147 predicted flux at the highest ULF power range (c). Below 30 nT²/Hz, ULF Pc5 influence on the lower
148 energy flux channels grows approximately linearly (d). The negative quadratic term describing the
149 influence of the upper range of ULF Pc5 is more pronounced when this wave is paired with VLF chorus in
150 the analysis (Figure 1A).

151 Increased VLF chorus has a positive influence on flux which is more pronounced when paired with EMIC
152 waves (Figure 1 A and C, Table 1 and 3; letter e). When paired with ULF Pc5 waves, the positive VLF
153 chorus effect on higher energies is explained mostly by the squared (nonlinear) term as shown by the
154 significant effects of Chorus² in Table 1 compared to the nonsignificant linear effects of Chorus.

155 EMIC waves show an increasingly negative, mostly linear effect at higher flux energies (Figure 1 B and C;
156 letter f). Quadratic effects of EMIC waves are not statistically significant except at the lowest energy
157 and when paired with ULF Pc5 (EMIC² term of Tables 2 and 3).

158 Waves interact synergistically in some situations. ULF Pc5 and VLF chorus mutually increase their effects
159 (ULF Pc5 X Chorus terms of Table 1). This interaction is statistically significant at higher flux energies
160 (3.5-7.8 MeV; terms where $p < .05$). ULF Pc5 and EMIC waves tend to depress the other's effect at the
161 two lower channels of flux (Table 2: negative ULF Pc5 X EMIC interaction term at 0.7-1.8 and 1.8-3.5
162 MeV). In Figure 1B EMIC waves act to reduce low energy electron fluxes in the presence of high ULF Pc5
163 wave intensities. They appear to act in synergy with ULF Pc5 waves at the highest energy electron
164 channels (3.5-7.8 MeV), but this effect is not statistically significant (ULF Pc5 X EMIC terms of Table 2).
165 In Figure 1C the EMIC waves act to quench the positive influence of increasing VLF chorus intensities,
166 although this quenching action becomes less effective in the higher energy channels (negative EMIC X
167 Chorus terms of Table 3).

168 **3.1 Wave effects during quiet vs. disturbed times**

169 To study whether wave effects during geomagnetically quiet days are different than on disturbed days,
170 we performed the same regression analyses as above, but with data separated into low Kp (<2.3 (2+),
171 lowest 75th percentile of daily averages) vs. high Kp (> 2.3 (2+), highest 25th percentile of daily averages)
172 (Figures 2, 3, and 4). The effects of wave intensity variations during quiet times are less influential. This
173 may in part be because of a lower range of observed intensities during low Kp. In less disturbed times
174 the ULF Pc5 index varies from 0 – 40 nT²/Hz instead of 0 – 125 nT²/Hz at high Kp. VLF chorus also
175 exhibits a lower dynamic range during quiet periods to a range of -2.5 – 1 log($\mu\text{V}^2/\text{m}^2/\text{Hz}$) vs. -2 –
176 1.75 during high Kp. However, the range in the number of hours high power EMIC waves are observed
177 is higher during quiet periods, with EMIC activity occurring up to 14 h/day instead of up to 11 h/day
178 during high Kp. These differences in predictor ranges may affect the response of flux, most dramatically
179 to the expanded ULF Pc5 range during disturbed times. However, it is also possible that this reflects
180 changes in the ionosphere which influences detection of EMIC waves in the ground-based data.

181 The response of flux at low Kp to ULF Pc5 waves is always positive (e.g., letter a, Figures 2 and 3), while
182 at high Kp electron flux peaks during midrange ULF Pc5 values as it does in the full data set (b).
183 However, the greater range of ULF Pc5 under high Kp conditions is not entirely responsible for the

184 higher flux response. In the lowest energy channel (0.7-1.8 MeV) the response of flux to ULF Pc5 is
185 higher even in the 0-40 nT²/Hz range of the ULF Pc5 index when Kp is high.

186 At low Kp, when VLF chorus is paired with ULF Pc5, the linear flux response is mostly positive over the
187 energy levels (e.g., Figure 2, letter c), but a negative square term (quadratic effect) causes a levelling off
188 of the response (a downward trend) as VLF chorus increases (e.g., letter d of Figure 2). This response is
189 most visible at 0.7-1.8 MeV. However, at high Kp, while the response to VLF chorus is linear at the lower
190 energies (e), the positive square term (quadratic) at the higher energies becomes more influential (f),
191 describing a more intense response to VLF chorus. This same general pattern is seen when VLF chorus is
192 paired with EMIC waves (Figure 4).

193 At low Kp, the negative response of electron flux levels to EMIC waves is weak, with lower energies even
194 showing a positive response (Figures 3 and 4, letter g).

195 The high Kp response for all three wave types is close to that seen in the full analysis. Most of the effect
196 of waves in the full analysis is thus due to what occurs during disturbed conditions, but analyzing the
197 high Kp days separately shows an even stronger flux response to wave effects. The lowest energy
198 channel (0.7-1.8 MeV) shows a high flux at high Kp even at the lowest wave activity. This indicates that
199 higher fluxes in this energy range are mainly due to additional processes occurring during disturbed
200 times and not necessarily to these waves alone.

201 **3.2 Wave Effects during southward vs. northward Bz**

202 As EMIC waves do not show dramatic nonlinear or interactive effects, we present only the ULF Pc5 X VLF
203 Chorus model split by southward vs. northward daily averaged IMF Bz (Figure 5). Under conditions of
204 more southward Bz, ULF Pc5 waves are more effective at enhancing flux in the lowest energy channels.
205 This effect drops off at the higher energies. Even high values of ULF Pc5 result in increased flux at the
206 lowest energy as the negative quadratic effect does not contribute appreciably. However, midrange
207 values of ULF Pc5 wave intensity increase higher energy flux more than the highest values of ULF Pc5
208 intensity. During northward Bz, the nonlinear negative effect of ULF Pc5 is stronger than during
209 southward Bz. Increases in ULF Pc5 result in lowering of flux.

210 Increased VLF chorus results in increased flux at all energy levels during southward Bz, with the
211 increases becoming more nonlinear with increased electron energy. During northward Bz, there is little
212 effect of VLF chorus when ULF Pc5 is weak. However, as in our previous analysis, when the ULF Pc5
213 wave intensity is ~ 60 nT²/Hz VLF chorus waves act to increase electron flux levels, particularly for the
214 lower energy channels.

215

216 **4. Discussion**

217 In a previous paper, we studied the combined linear effects of ULF Pc5, VLF chorus, and EMIC waves on
218 log₁₀ flux of geosynchronous orbit relativistic trapped electrons (Simms et al., 2018a submitted (Paper
219 1)). In the present paper, we further this exploration by investigating the non-linear effects of these
220 waves, as well as possible synergistic interactions between pairs of wave types.

221 At all four of the energy levels studied, ULF Pc5 power is most influential when its index is at mid-range
222 values. Its influence on flux levels falls off at the highest values of the index as the negative non-linear

223 quadratic term in the regression model becomes more influential. At the lower flux energies in
224 particular (0.7-3.5 MeV), the non-linear response of flux to ULF Pc5 waves could mean that a strictly
225 linear model would find no observed correlation with flux if a wide range of ULF Pc5 values are
226 considered. Positive correlations with flux may only be found if ULF Pc5 waves are restricted to the
227 lower to mid-range values. This could account for conflicting results in correlations of ULF Pc5 waves
228 with flux in earlier studies.

229 ULF Pc5 waves have been predicted to contribute to electron loss by outward radial diffusion during
230 shock events (Brautigam & Albert, 2000; Degeling et al., 2008; Hudson et al., 2014; Loto'aniu et al.,
231 2010; Shprits et al., 2006; Ukhorskiy et al., 2009; Zong et al., 2012). Although linear regression models in
232 our previous paper only showed evidence of flux enhancement by ULF Pc5 waves and no loss (Simms et
233 al., 2018a submitted (Paper 1)), the nonlinear terms in our present study show that the upper range of
234 ULF Pc5 intensities leads to reduced flux, in accord with the above studies. In our present study, ULF Pc5
235 induced loss is most prominent at energies >3.5 MeV. Acceleration is mainly accomplished by moderate
236 ULF Pc5 activity ($\sim 60 \text{ nT}^2/\text{Hz}$ in this study), and mostly into energies between 0.7 and 3.5 MeV.

237 Non-linear effects of VLF chorus are more modest, but positive. This results in more flux at the highest
238 intensity ranges of chorus than would be expected from a strictly linear model. This has been predicted
239 by test-particle modelling investigating the effect of large amplitude chorus (Bortnik et al., 2008; Cattell
240 et al., 2008). VLF chorus appears more influential when ULF Pc5 is not also included in the model. This
241 may be due to chorus (when ULF Pc5 is not present) representing the ULF Pc5 effects due to the high
242 correlation between the two wave types. VLF chorus is most influential on the lower energy relativistic
243 electrons. Its reduced effect on higher energies may result from chorus also driving the compensating
244 effect of precipitation of the most energetic electrons (Bortnik et al., 2006; Bortnik & Thorne, 2007;
245 Hikishima et al., 2010; Lam et al., 2010; Lorentzen et al., 2001; Millan & Thorne 2007; Orlova & Shprits,
246 2010).

247 Ozeke et al. (2017) have postulated that VLF chorus does not contribute to increased flux, as their
248 model, using ULF wave diffusion, can adequately explain flux levels on the basis of ULF Pc5 waves alone.
249 Jaynes et al. (2015) argued that chorus is the primary driver, at least after a depletion event. Our results
250 show that both waves contribute to flux enhancements. Although one or the other may dominate as
251 the primary driver in individual events, in general, we find that enhancements are driven by both waves
252 in combination, both additively, and, at the higher energy levels, synergistically. Previous work has
253 shown that VLF chorus and ULF Pc5 effects at geostationary orbit may add to enhance electron flux
254 (O'Brien et al., 2003). However, the significant interaction term we see in our regression models shows
255 that their combined action is not just additive but synergistic as well. Higher chorus levels result in more
256 effective enhancement by mid-range ULF Pc5, and vice versa. The highest flux levels are seen at high
257 chorus intensity levels and mid-range ULF Pc5 index levels. This may be the result of ULF Pc5 waves,
258 through radial diffusion, pre-accelerating electrons to sub-relativistic energies. Once these electrons are
259 at this energy level, VLF chorus waves are more effective at accelerating them to relativistic speeds.

260 The nonlinearity of the ULF Pc5 influence may be responsible for differing conclusions in the literature
261 about its effectiveness relative to VLF chorus. Our results show that if ULF Pc5 occurs at low to moderate
262 levels in a given study, a positive linear relationship between it and flux will be found. However, the
263 inclusion of the upper range of ULF Pc5 levels in another study could lead to the conclusion that there is
264 a negative relationship or none at all, leaving VLF chorus as the only likely seeming driver. It is also

265 noteworthy that combining ULF Pc5 and VLF chorus in the same model results in a stronger negative
266 effect of high intensity ULF Pc5 in the higher energy ranges. Thus, the addition of VLF chorus allows the
267 observation of the negative ULF Pc5 quadratic effect. This demonstrates that the correlations and
268 interactions between wave types means studying one in isolation may not lead to valid physical
269 interpretations of its effects. Models of these wave effects on flux on flux may benefit from using
270 several waves as predictors and including the non-linear quadratic effects as well as the synergistic
271 effects between the waves.

272 For the most part, EMIC waves show both a less pronounced linear influence and a smaller nonlinear
273 effect on flux. However, they do show a negative interaction with both ULF Pc5 and chorus at the lower
274 energy levels. This negative synergism results in a larger decrease in flux when both EMIC and either
275 ULF Pc5 or chorus waves are at high levels. Modelling work has suggested that loss processes associated
276 with chorus could act most effectively in conjunction with EMIC waves (Mourenas et al., 2016; Summers
277 & Ma, 2000). There is also observational evidence that the EMIC and chorus/hiss waves act additively to
278 decrease flux (Zhang et al., 2017). The negative interaction found in our regression models shows that
279 the combined effect of EMIC and VLF chorus waves is not just additive. High levels of one enhance the
280 negative action of the other. We have also found that loss due to ULF Pc5 (at high levels) is enhanced in
281 the presence of EMIC waves in a multiplicative and not just additive manner.

282 The effect of all types of waves during quiet times ($K_p < 2.3$) is modest, while that during disturbed times
283 more closely follows the patterns seen overall. Thus, most of the effects in the full analysis are due to
284 the disturbed condition response. Some of the response difference between quiet and disturbed
285 geomagnetic activity levels is due to different ranges of wave intensity present in these differing times.
286 In particular, the negative non-linear response to high levels of ULF Pc5 cannot be observed during quiet
287 times because this wave type does not show the same high level of activity as it does during disturbed
288 conditions. However, the initial linear slope of the low intensity ULF Pc5 effect at high K_p is steeper than
289 that during low K_p ; thus, the effect of the same level of ULF Pc5 activity is greater during disturbed
290 times. The same is true for VLF chorus. Chorus also shows a levelling off of effect at higher activity (> 0
291 $\log(\mu V^2/m^2/Hz)$) during quiet times. This may indicate that precipitation due to chorus is a larger
292 factor during quiet times.

293 Ground stations detect EMIC waves at a large range of L shells due to ionospheric ducting. Thus, ground
294 data from Halley ($L = 4.6$) is useful in this study because it only includes wave activity at
295 geosynchronous orbit (Anderson et al., 1992; Kim et al., 2010, 2011). However, long distance
296 ionospheric ducting of EMIC waves is disrupted during disturbed times. These waves are less likely to be
297 observed on the ground during these periods (Engebretson et al., 2008). Our study confirms this:
298 ground-observed EMIC waves (at Halley) occur over more hours (up to 14 hrs/day) during quiet times
299 than they do during disturbed conditions (only up to 10 hrs/day). Satellite observations, on the other
300 hand, show a positive association between disturbed times and increased EMIC activity (Keika et al.,
301 2013). This may complicate interpretations of correlations between ground-based EMIC observations
302 and electron flux at geosynchronous orbit.

303 At high K_p , flux is high in the lowest energy channel (0.7-1.8 MeV) even without wave enhancements. It
304 is likely that substorm and magnetic activity alone are responsible for much of the flux enhancements
305 during disturbed times.

306 VLF chorus has a positive effect during southward Bz, but a negative effect during northward Bz. This
307 agrees with previous findings that VLF chorus is more effective at accelerating electrons up to relativistic
308 energies during southward Bz (Miyoshi et al., 2013). We have found the same to be true of ULF Pc5
309 which is more effective at enhancing flux during southward Bz conditions. Southward Bz, when
310 reconnection is occurring, appears to be a necessary condition for the action of both VLF chorus and ULF
311 Pc5 waves on high energy electron flux.

312

313

314 **5. Summary**

315

316 We have undertaken a non-linear regression analysis of the LANL geostationary trapped \log_{10}
317 relativistic electron fluxes (0.7-7.8 MeV) in order to determine the influence of ULF Pc5, VLF and
318 EMIC wave intensities lagged by one day. We find that:

319

320 1. The response of relativistic electron flux levels to both ULF Pc5 and VLF chorus waves can be
321 nonlinear as well as linear. A quadratic model, therefore, may better predict flux response
322 to these waves.

323

324 2. ULF Pc5 waves contribute both to electron enhancement (at mid-range wave activity) and
325 loss (at high levels of wave intensity). The negative (nonlinear) response at high levels of
326 wave activity could lead to the conclusion that ULF Pc5 waves do not contribute to electron
327 enhancement in more simplistic regression models.

328

329 3. Nonlinear effects of VLF chorus are positive. Electron flux response at high levels of chorus
330 intensity is higher than would be predicted by a strictly linear model.

331

332 4. Synergistic interaction effects between some wave types are shown to be important. High
333 levels of VLF chorus intensity and mid-range values of ULF Pc5 wave power result in more
334 electron acceleration than would be predicted by an additive model.

335

336 5. The negative effect of EMIC waves on flux (linked to flux decreases) is more pronounced
337 than would be predicted by an additive linear model when combined with either chorus or
338 ULF Pc5 waves.

339

340 6. Flux response to ULF Pc5 and VLF chorus waves varies by geomagnetic activity (Kp). During
341 disturbed conditions, flux responds more strongly to the same level of wave intensity. In
342 the lowest energy channel (0.7-1.8 MeV) flux at high Kp is at a high level even without wave
343 activity enhancement.

344

345 7. Flux response to ULF Pc5 and VLF chorus waves is stronger during southward Bz conditions.

346

347 8. Unstandardized regression coefficients for models incorporating these nonlinear and
348 synergistic effects are presented (Tables 1-3) for use in modelling.

349

350

351

352

353

354 **Acknowledgements**

355 We thank J. Bortnik, Y. Shprits, T.P. O'Brien and an anonymous reviewer for their comments on a
356 previous draft of this work, M. Ohnsted and N. Capman for EMIC wave identification, and R. Gamble for
357 preparing and J.-J. Berthelier (PI) for providing DEMETER ICE data. Relativistic, seed, and source electron
358 flux data were obtained from Los Alamos National Laboratory (LANL) geosynchronous energetic particle
359 instruments (contact: G. D. Reeves). The ULF index is available at <http://ulf.gcras.ru/>. IMF Bz, Dst, and
360 solar wind V, N, and P data are available from Goddard Space Flight Center Space Physics Data Facility at
361 the OMNIWeb data website (http://omniweb.gsfc.nasa.gov/html/ow_data.html). Work at Augsburg
362 University was supported by NSF grants AGS-1264146, PLR-1341493, and AGS- 1651263.

363

364

365 **References**

366 Anderson, B. J., Erlandson, R.E., & Zanetti, L. J. (1992), A statistical study of Pc 1-2 magnetic
367 pulsations in the equatorial magnetosphere. 1. Equatorial occurrence distributions, *Journal of*
368 *Geophysical Research*, 97, 3075–3088, doi:10.1029/91JA02706

369 Berthelier, J.J., Godefroy, M., Leblanc, F., Malingre, M., Menvielle, M., Lagoutte, D., Brochot, J.
370 Y., Colin, F., Elie, F., Legendre, C., Zamora, P., Benoist, D., Chapuis, Y., Artru, J., Pfaff R. (2006), ICE, the
371 electric field experiment on DEMETER, *Planetary and Space Science*, 54, 456–471,
372 doi:10.1016/j.pss.2005.10.016

373 Blum, L. W., Halford, A., Millan, R., Bonnell, J.W., Goldstein, J., Usanova, M., Engebretson, M.,
374 Ohnsted, M., Reeves, G., Singer, H., Clilverd, M., and Li, X. (2015), Observations of coincident EMIC wave
375 activity and duskside energetic electron precipitation on 18–19 January 2013, *Geophysical Research*
376 *Letters*, 42, 5727–5735, doi:10.1002/2015GL065245

377 Borovsky, J. E. & Denton, M.H. (2014), Exploring the cross correlations and autocorrelations of
378 the ULF indices and incorporating the ULF indices into the systems science of the solar wind-driven
379 magnetosphere, *Journal of Geophysical Research*, 10.1002/2014JA019876

380 Bortnik, J., Thorne, R. M., O'Brien, T.P., Green, J.C., Strangeway, R.J., Shprits, Y.Y., & Baker, D.N.
381 (2006), Observation of two distinct, rapid loss mechanisms during the 20 November 2003 radiation belt
382 dropout event, *Journal of Geophysical Research*, 111, A12216, doi:10.1029/2006JA011802

383 Bortnik, J. & Thorne, R.M. (2007), The dual role of ELF/VLF chorus waves in the acceleration and
384 precipitation of radiation belt electrons, *Journal of Atmospheric and Solar-Terrestrial Physics*, 69 (2007)
385 378–386, doi:10.1016/j.jastp.2006.05.030

386 Bortnik, J., Thorne, R.M., & Inan, U.S. (2008), Nonlinear interaction of energetic electrons with
387 large amplitude chorus, *Geophysical Research Letters*, 35, L21102, doi:10.1029/2008GL035500

388 Brautigam, D. H. & Albert, J.M. (2000), Radial diffusion analysis of outer radiation belt electrons
389 during the October 9, 1990, magnetic storm, *Journal of Geophysical Research*, 105, 291-309, doi:
390 10.1029/1999JA900344

391 Cattell, C., Wygant, J.R., Goetz, K., Kersten, K., Kellogg, P.J., von Rosenvinge, T.,
392 Bale, S.D., Roth, I., Temerin, M., Hudson, M. K., Mewaldt, R.A., Wiedenbeck, M.,
393 Maksimovic, M., Ergun, R., Acuna, M., & Russell, C.T. (2008), Discovery of very large amplitude whistler-
394 mode waves in Earth's radiation belts, *Geophysical Research Letters*, 35, L01105,
395 doi:10.1029/2007GL032009

396
397 Clilverd, M. A., Rodger, C.J., Millan, R. M., Sample, J.G., Kokorowski, M., McCarthy, M.P., Ulich,
398 T., Raita, T., Kavanagh, A.J., & Spanswick, E. (2007), Energetic particle precipitation into the middle
399 atmosphere triggered by a coronal mass ejection, *Journal of Geophysical Research*, 112, A12206,
400 doi:10.1029/2007JA012395

401 Clilverd, M. A., Duthie, R., Hardman, R., Hendry, A.T., Rodger, C.J., Raita, T., Engebretson, M.,
402 Lessard, M.R., Danskin, D., & Milling, D.K. (2015), Electron precipitation from EMIC waves: A case study
403 from 31 May 2013, *Journal of Geophysical Research Space Physics*, 120, 3618–3631,
404 doi:10.1002/2015JA021090

405 Cowles, M. & Davis, C. (1982), On the origins of the .05 level of statistical significance, *American*
406 *Psychologist*, 37(5), 553-558.

407 Degeling, A. W., Ozeke, L.G., Rankin, R., Mann, I.R., & Kabin, K. (2008), Drift resonant generation
408 of peaked relativistic electron distributions by Pc 5 ULF waves, *Journal of Geophysical Research*, 113,
409 A02208, doi:10.1029/2007JA012411

410 Degtyarev, V.I., Kharchenko, I.P., Potapov, A.S., Tsegmed, B., & Chudnenko, S.E. (2009),
411 Qualitative estimation of magnetic storm efficiency in producing relativistic electron flux in the Earth's
412 outer radiation belt using geomagnetic pulsations data, *Advances in Space Research*, 43, 829–836,
413 doi:10.1016/j.asr.2008.07.004

414 Engebretson, M. J., Lessard, M.R., Bortnik, J., Green, J.C., Horne, R.B., Detrick, D.L., Weatherwax,
415 A.T., Manninen, J., Petit, N.J., Posch, J.L., & Rose, M.C. (2008), Pc1-Pc2 waves and energetic particle
416 precipitation during and after magnetic storms: Superposed epoch analysis and case studies, *Journal of*
417 *Geophysical Research*, 113, A01211, doi:10.1029/2007JA012362

418
419 Engebretson, M. J., Posch, J.L., Wygant, J.R., Kletzing, C.A., Lessard, M.R., Huang, C.-L., Spence,
420 H.E., Smith, C.W., Singer, H.J., Omura, Y., Horne, R.B., Reeves, G.D., Baker, D.N., Gkioulidou, M., Oksavik,
421 K., Mann, I.R., Raita, T., & Shiokawa, K. (2015), Van Allen probes, NOAA, GOES, and ground observations

422 of an intense EMIC wave event extending over 12 h in magnetic local time, *Journal of Geophysical*
423 *Research Space Physics*, 120,doi:10.1002/2015JA021227

424 Gao, X., Li, W., J. Bortnik, J., Thorne, R.M., Lu, Q., Ma, Q., Tao, X., & Wang, S. (2015), The effect
425 of different solar wind parameters upon significant relativistic electron flux dropouts in the
426 magnetosphere, *Journal of Geophysical Research Space Physics*, 120,4324–4337,
427 doi:10.1002/2015JA021182

428 Hikishima, M., Omura, Y., & Summers, D. (2010), Microburst precipitation of energetic electrons
429 associated with chorus wave generation, *Geophysical Research Letters*, 37, L07103,
430 doi:10.1029/2010GL042678.

431 Horne, R. B., Thorne, R.M., Glauert, S.A., Albert, J.M., Meredith, N.P., & Anderson, R. R. (2005),
432 Timescale for radiation belt electron acceleration by whistler mode chorus waves, *Journal of*
433 *Geophysical Research*, 110, A03225, doi:10.1029/2004JA010811

434 Hudson, M. K., Baker, D.N., Goldstein, J., Kress, B.T., Paral, J., Toffoletto, F.R., & Wiltberger, M.
435 (2014), Simulated magnetopause losses and Van Allen Probe flux dropouts, *Geophysical Research*
436 *Letters*, 41, 1113–1118, doi:10.1002/2014GL059222

437 Iles, H.A., Meredith, N.P., Fazakerley, A.N., & Horne, R.B. (2006), Phase space density analysis of
438 the outer radiation belt energetic electron dynamics, *Journal of Geophysical Research*, 111, A03204,
439 doi:10.1029/2005JA011206

440 Jaynes, A. N., Baker, D.N., Singer, H.J., Rodriguez, J.V., Loto'aniu, T.M., Ali, A.F., Elkington, S.R., Li,
441 X., Kanekal, S.G., Fennell, J.F., Li, W., Thorne, R.M., Kletzing, C.A., Spence, H.E., & Reeves, G.D. (2015),
442 Source and seed populations for relativistic electrons: Their roles in radiation belt changes, *Journal of*
443 *Geophysical Research Space Physics*, 120, 7240–7254, doi:10.1002/2015JA021234

444 Keika, K., Takahashi, K., Ukhorskiy, A.Y., & Miyoshi, Y. (2013), Global characteristics of
445 electromagnetic ion cyclotron waves: Occurrence rate and its storm dependence, *Journal of Geophysical*
446 *Research Space Physics*, 118, 4135–4150, doi:10.1002/jgra.50385

447
448 Kim, H., Lessard, M.R., Engebretson, M.J., & Lühr, H. (2010), Ducting characteristics of Pc 1
449 waves at high latitudes on the ground and in space, *Journal of Geophysical Research*, 115, A09310,
450 doi:10.1029/2010JA015323

451 Kim, H., Lessard, M.R., Engebretson, M.J., & Young, M.A. (2011), Statistical study of Pc 1-2 wave
452 propagation characteristics in the high-latitude ionospheric waveguide, *Journal of Geophysical Research*,
453 116, A077227, doi:10.1029/2010JA016355, 2011

454 Kozyreva, O., V. Pilipenko, V., Engebretson, M.J., Yumoto, K., Watermann, J., & Romanova, N.
455 (2007), In search of a new ULF wave index: Comparison of Pc5 power with dynamics of geostationary
456 relativistic electrons, *Planetary and Space Science*, 55, 755–769.

457 Lam, M. M. Horne, R.B., Meredith, N.P., Glauert, S.A., Moffat-Griffin, T., & Green, J.C. (2010),
458 Origin of energetic electron precipitation >30 keV into the atmosphere, *Journal of Geophysical Research*,
459 115, A00F08, doi:10.1029/2009JA014619

460 Lam, H.-L. (2017), On the predictive potential of Pc5 ULF waves to forecast relativistic electrons
461 based on their relationships over two solar cycles, *Space Weather*, 15, 163–179,
462 doi:10.1002/2016SW001492

463 Li, L. Y., Cao, J.B., Zhou, G.C., & Li, X. (2009), Statistical roles of storms and substorms in changing
464 the entire outer zone relativistic electron population, *J. Geophys. Res.*, 114, A12214,
465 doi:10.1029/2009JA01433

466 Li, Z., Millan, R.M., Hudson, M.K., Woodger, L.A., Smith, D.M., Chen, Y., Friedel, R., Rodriguez,
467 J.V., Engebretson, M.J., Goldstein, J., Fennell, J.F., & Harlan E. Spence, H.E. (2014), Investigation of EMIC
468 wave scattering as the cause for the BARREL 17 January 2013 relativistic electron precipitation event: A
469 quantitative comparison of simulation with observations, *Geophysical Research Letters*, 41, 8722–
470 8729, doi:10.1002/2014GL062273

471 Lorentzen, K. R., Blake, J.B., Inan, U.S., & Bortnik, J. (2001), Observations of relativistic electron
472 microbursts in association with VLF chorus, *Journal of Geophysical Research*, 106, 6017.

473 Loto'aniu, T.M., Singer, H.J., Waters, C.L., Angelopoulos, V., Mann, I.R., Elkington, S.R., &
474 Bonnell, J.W. (2010), Relativistic electron loss due to ultralow frequency waves and enhanced outward
475 radial diffusion, *Journal of Geophysical Research*, 115, A12245, doi:10.1029/2010JA015755

476 Mann, I. R., O'Brien, T.P., & Milling, D.K. (2004), Correlations between ULF wave power, solar
477 wind speed, and relativistic electron flux in the magnetosphere: solar cycle dependence, *Journal of*
478 *Atmospheric and Solar Terrestrial Physics*, 66, 187-198/j.jastp.2003.10.002.

479 Mathie, R. A. & Mann, I.R. (2000), A correlation between extended intervals of ULF wave power
480 and storm-time geosynchronous electron flux enhancements, *Geophys. Res. Lett.*, 27, 3261-3264.

481 Meredith, N. P., Horne, R.B., Iles, R.H.A., Thorne, R.M., Heynderickx, D., & Anderson, R.R. (2002),
482 Outer zone relativistic electron acceleration associated with substorm-enhanced whistler mode chorus,
483 *Journal of Geophysical Research*, 107(A7), 1144, doi:10.1029/2001JA900146

484 Meredith, N. P., Cain, M., Horne, R.B., Thorne, R.M., Summers, D., & Anderson, R.R. (2003),
485 Evidence for chorus-driven electron acceleration to relativistic energies from a survey of
486 geomagnetically disturbed periods, *Journal of Geophysical Research*, 108, 1248,
487 doi:10.1029/2002JA009764

488 Millan, R.M. & Thorne, R.M. (2007), Review of radiation belt relativistic electron losses, *Journal*
489 *of Atmospheric and Solar-Terrestrial Physics*, 69 (2007) 362–377, doi:10.1016/j.jastp.2006.06.019

490 Miyoshi, Y., Morioka, A., Obara, T., Misawa, H., Nagai, T., & Kasahara, Y. (2003), Rebuilding
491 process of the outer radiation belt during the 3 November 1993 magnetic storm: NOAA and Exos-D
492 observations, *Journal of Geophysical Research*, 108, NO. A1, 1004, doi:10.1029/2001JA007542

493 Miyoshi, Y., Morioka, A., Kataoka, R., Kasahara, Y., & Mukai, T. (2007), Evolution of the outer
494 radiation belt during the November 1993 storms driven by corotating interaction regions, *Journal of*
495 *Geophysical Research*, 112, A05210, doi:10.1029/2006JA012148

496 Miyoshi, Y., Sakaguchi, K., Shiokawa, K., Evans, D., Albert, J., Connors, M., & Jordanova, V.
497 (2008), Precipitation of radiation belt electrons by EMIC waves, observed from ground and space,
498 *Geophysical Research Letters*, 35, L23101, doi:10.1029/2008GL035727

499 Miyoshi, Y., Kataoka, R., Kasahara, Y., Kumamoto, A., Nagai, T., & Thomsen, M.F. (2013), High-
500 speed solar wind with southward interplanetary magnetic field causes relativistic electron flux
501 enhancement of the outer radiation belt via enhanced condition of whistler waves, *Geophysical*
502 *Research Letters*, 40, doi:10.1002/grl.50916

503 Mourenas, D., Artemyev, A.V., Ma, Q., Agapitov, O.V., & Li, W. (2016), Fast dropouts of multi-
504 MeV electrons due to combined effects of EMIC and whistler mode waves, *Geophysical Research*
505 *Letters*, 43, 4155–4163, doi:10.1002/2016GL068921

506
507 Neter, J., Wasserman, W., & Kutner, M.H. (1985), *Applied Linear Statistical Models*, Richard D.
508 Irwin, Inc., Homewood, Ill., 1127 pp.

509 O'Brien, T. P., Lorentzen, K. R., Mann, I.R., Meredith, N.P., Blake, J.B., Fennell, J.F., Looper, M.D.,
510 Milling, D.K., & Anderson, R.R. (2003), Energization of relativistic electrons in the presence of ULF power
511 and MeV microbursts: Evidence for dual ULF and VLF acceleration, *Journal of Geophysical Research*, 108,
512 1329, doi:10.1029/2002JA009784

513 Orlova, K. G. & Shprits, Y.Y. (2010), Dependence of pitch - angle scattering rates and loss
514 timescales on the magnetic field model, *Geophysical Research Letters*, 37, L05105,
515 doi:10.1029/2009GL041639

516 Ozeke, L. G., Mann, I. R., Murphy, K.R., Sibeck, D.G., & Baker, D.N. (2017), Ultra-relativistic
517 radiation belt extinction and ULF wave radial diffusion: Modeling the September 2014 extended dropout
518 event, *Geophysical Research Letters*, 44, doi:10.1002/2017GL072811

519 Rodger, C. J., Raita, T., Clilverd, M.A., Seppälä, A., Dietrich, S., Thomson, N.R., & Ulich, T. (2008),
520 Observations of relativistic electron precipitation from the radiation belts driven by EMIC waves,
521 *Geophysical Research Letters*, 35, L16106, doi:10.1029/2008GL034804

522 Rostoker, G., Skone, S., & Baker, D.N. (1998), On the origin of relativistic electrons in the
523 magnetosphere associated with some geomagnetic storms, *Geophysical Research Letters*, 25, doi:
524 10.1029/98GL02801

525 Shprits, Y.Y., Thorne, R.M., Friedel, R., Reeves, G.D., Fennell, J., Baker, D.N., & Kanekal, S.G.
526 (2006), Outward radial diffusion driven by losses at magnetopause, *Journal of Geophysical Research*,
527 111, A11214, doi:10.1029/2006JA011657

528 Simms, L. E., Engebretson, M.J., Pilipenko, V., Reeves, G.D., & Clilverd, M. (2016), Empirical
529 predictive models of daily relativistic electron flux at geostationary orbit: Multiple regression analysis,
530 *Journal of Geophysical Research Space Physics*, 121, 3181–3197, doi:10.1002/2016JA022414

531 Simms, L. E., Engebretson, M.J., Clilverd, M., Rodger, C., Lessard, M., Gjerloev, J., & Reeves, G.
532 2018a (Paper 1)), A distributed lag-autoregressive model of geostationary relativistic electron fluxes:
533 Comparing the influences of ULF Pc5, VLF chorus, EMIC, seed and source electrons, solar wind
534 compression, and substorms, submitted.

535 Spasojevic, M. & Inan, U.S. (2005), Ground based VLF observations near L = 2.5 during the
536 Halloween 2003 storm, *Geophysical Research Letters*, 32, L21103, doi:10.1029/2005GL024377

537 Su, Z., Zhu, H., Xiao, F., Zong, Q.-G., Zhou, X.-Z., Zheng, H., Wang, Y., Wang, S., Hao, Y.-X., Gao, Z.,
538 He, Z., Baker, D.N., Spence, H.E., Reeves, G.D., Blake, J.B., & Wygant, J.R. (2015), Ultra-low-frequency
539 wave-driven diffusion of radiation belt relativistic electrons, *Nat. Comm.*, doi: 10.1038/ncomms10096

540 Summers, D. & Ma, C. (2000), Rapid acceleration of electrons in the magnetosphere by fast-
541 mode MHD waves, *Journal of Geophysical Research*, 105, 15,887-15895.

542 Summers, D. & Thorne, R.M. (2003), Relativistic electron pitch-angle scattering by
543 electromagnetic ion cyclotron waves during geomagnetic storms, *Journal of Geophysical Research*, 108,
544 NO. A4, 1143, doi:10.1029/2002JA009489

545 Thorne, R.M. (2010), Radiation belt dynamics: The importance of wave - particle interactions,
546 *Geophysical Research Letters*, 37, L22107, doi:10.1029/2010GL044990

547 Thorne, R. M., Li, W., Ni, B., Ma, Q., Bortnik, J., Chen, L., Baker, D.N., Spence, H.E., Reeves, G.D.,
548 Henderson, M.G., Kletzing, C.A., Kurth, W.S., Hospodarsky, G. B., Blake, J. B., Fennell, J.F., Claudepierre,
549 S.G., & Kanekal, S.G. (2013), Rapid local acceleration of relativistic radiation-belt electrons by
550 magnetospheric chorus, *Nature*, 504, 411, doi:10.1038/nature12889

551 Tsurutani, B. T. & Smith, E.J. (1977), Two types of magnetospheric ELF chorus and their substorm
552 dependences, *Journal of Geophysical Research*, 82, 5112-5128, doi: 10.1029/JA082i032p05112

553 Turner, D.L., Angelopoulos, V., Li, W., Hartinger, M.D., Usanova, M., Mann, I.R., Bortnik, J., &
554 Shprits, Y. (2013), On the storm-time evolution of relativistic electron phase space density in Earth's
555 outer radiation belt, *Journal of Geophysical Research: Space Physics*, 118, 2196–2212,
556 doi:10.1002/jgra.50151

557 Turner, D. L., Angelopoulos, V., Li, W., Bortnik, J., Ni, B., Ma, Q., Thorne, R.M., Morley, S.K.,
558 Henderson, M.G., Reeves, G.D., Usanova, M., Mann, I.R., Claudepierre, S.G., Blake, J.B., Baker, D.N.,
559 Huang, C.-L., Spence, H., Kurth, W., Kletzing, C., & Rodriguez, J.V. (2014), Competing source and loss
560 mechanisms due to wave-particle interactions in Earth's outer radiation belt during the 30 September to
561 3 October 2012 geomagnetic storm, *Journal of Geophysical Research Space Physics*, 119, 1960–1979,doi:
562 10.1002/2014JA019770

563 Ukhorskiy, A.Y., Sitnov, M.I., Takahashi, K., & Anderson, B.J. (2009), Radial transport of radiation
564 belt electrons due to stormtime Pc5 waves, *Ann. Geophys.*, 27, 2173–2181.

565 Usanova, M. E., Drozdov, A., Orlova, K., Mann, I.R., Shprits, Y., Robertson, M.T., Turner, D.L.,
566 Milling, D.K., Kale, A., Baker, D.N., Thaller, S.A., Reeves, G.D., Spence, H.E., Kletzing, C., & JWygant, J.
567 (2014), Effect of EMIC waves on relativistic and ultrarelativistic electron populations: Ground-based and
568 Van Allen Probes observations, *Geophysical Research Letters*, 41, 1375–1381,
569 doi:10.1002/2013GL059024

570 Zhang, X.-J., Mourenas, D., Artemyev, A.V., Angelopoulos, V., & Thorne, R.M. (2017),
571 Contemporaneous EMIC and whistler-Mode waves: observations and consequences for MeV electron
572 loss, *Geophysical Research Letters*, 44, 8113–8121, doi:10.1002/2017GL073886

573
574 Zong, Q.G., Wang, Y.F., Zhang, H., Fu, S.Y., Zhang, H., Wang, C.R., Yuan, C.J., & Vogiatzis, I.
575 (2012), Fast acceleration of inner magnetospheric hydrogen and oxygen ions by shock induced ULF
576 waves, *Journal of Geophysical Research*, 117, A11206, doi:10.1029/2012JA018024

577

578

579

580

581 Figure 1. Linear, non-linear, and synergistic effects between pairs of wave types. A. ULF Pc5 and VLF
582 chorus, B. ULF Pc5 and EMIC, C. EMIC and VLF chorus. Autoregressive lag 1 models include squared and
583 multiplicative terms that test the non-linearity and interactive effects, respectively, for ULF Pc5 power
584 (nT^2/Hz), lower band VLF chorus intensity ($\log(\mu V^2/m^2/\text{Hz})$), and EMIC (the number of hours per
585 day during which there was high EMIC activity ($> 10^{-3} nT^2 \text{ Hz}$) in the $<1 \text{ Hz}$ band) waves on relativistic
586 electron flux (z-axis: $\log(\text{electrons}/(\text{cm}^2/\text{s}/\text{sr}/\text{keV}))$).

587 Figure 2. Linear, non-linear, and synergistic effects of ULF Pc5 and VLF chorus waves during A. quiet -
588 low Kp (< 2.3 , lower 75th percentile) and B. disturbed - high Kp (>2.3 , upper 25th percentile).
589 Autoregressive lag 1 models include squared and multiplicative terms that test the nonlinear and
590 interactive effects.

591 Figure 3. Linear, non-linear, and synergistic effects of ULF Pc5 and EMIC waves during A. quiet - low Kp
592 (< 2.3 , lower 75th percentile) and B. disturbed - high Kp (>2.3 , upper 25th percentile). Autoregressive lag
593 1 models include squared and multiplicative terms that test the nonlinear and interactive effects.

594 Figure 4. Linear, non-linear, and synergistic effects of EMIC and VLF chorus waves during A. quiet - low
595 Kp (< 2.3 , lower 75th percentile) and B. disturbed - high Kp (>2.3 , upper 25th percentile). Autoregressive
596 lag 1 models include squared and multiplicative terms that test the nonlinear and interactive effects.

597 Figure 5. Linear, non-linear, and synergistic effects of ULF Pc5 and VLF chorus waves during A.
598 southward Bz (daily average of Bz < -0.3), B. northward Bz (daily average Bz > 0.5). Autoregressive lag 1
599 models include squared and multiplicative terms that test the nonlinear and interactive effects.

600

601

602

603

604 Table 1. Unstandardized regression coefficients of the ULF Pc5 X Chorus model. All predictors are lag 1
 605 (measured one day before flux). N=1534 days. *: effect is statistically significant ($p < 0.05$).

606

	0.7-1.8 MeV	1.8-3.5 MeV	3.5-6.0 MeV	6.0-7.8 MeV
Intercept	.166390*	-.239262*	-.405719*	-.358266*
ULF Pc5	.014519*	.020247*	.018550*	.006877*
Chorus	.052503	.102895	.038928	.017680
ULF Pc5 ²	-.000106*	-.000160*	-.000176*	-.000069*
Chorus ²	-.019033	.004751	.035591*	.016232*
ULF Pc5 X Chorus	.000611	.001900	.004420*	.001946*
Lag1 Flux (AR term)	.774144*	.788388*	.896287*	.829303*

607

608

609

610 Table 2. Unstandardized regression coefficients of the ULF Pc5 X EMIC model. All predictors are lag 1
 611 (measured one day before flux). N= 1475 days. *: effect is statistically significant ($p < 0.05$).

612

	0.7-1.8 MeV	1.8-3.5 MeV	3.5-6.0 MeV	6.0-7.8 MeV
Intercept	-.074965*	-.452816*	-.349185*	-.320530*
ULF Pc5	.022413*	.028532*	.016394*	.005195*
EMIC	.019205*	.009558	-.035587*	-.011929*
ULF Pc5 ²	-.000141*	-.000164*	-.000079*	-.000020*
EMIC ²	-.002066*	-.001424	.001171	-.000083
ULF Pc5 X EMIC	-.000802*	-.000976*	-.000111	.000145
Lag1 Flux (AR term)	.811735*	.816074*	.917664*	.844721*

613

614

615

616 Table 3. Unstandardized regression coefficients of the EMIC X Chorus model. All predictors are lag 1
 617 (measured one day before flux). N= 1375 days. *: effect is statistically significant (p < 0.05).

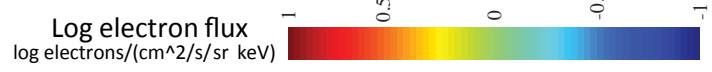
618

	0.7-1.8 MeV	1.8-3.5 MeV	3.5-6.0 MeV	6.0-7.8 MeV
Intercept	.505595*	.243309*	.055587*	-.186412*
EMIC	-.026310*	-.038423*	-.044165*	-.008977
Chorus	.208823*	.329763*	.280662*	.111863*
EMIC^2	-.000858	-.000390	.001046	-.000287
Chorus^2	-.008829	.025636*	.067326*	.030831*
EMIC X Chorus	-.020428*	-.019829*	-.006749	-.000572
Lag1 Flux (AR term)	.784324*	.805480*	.918211*	.843477

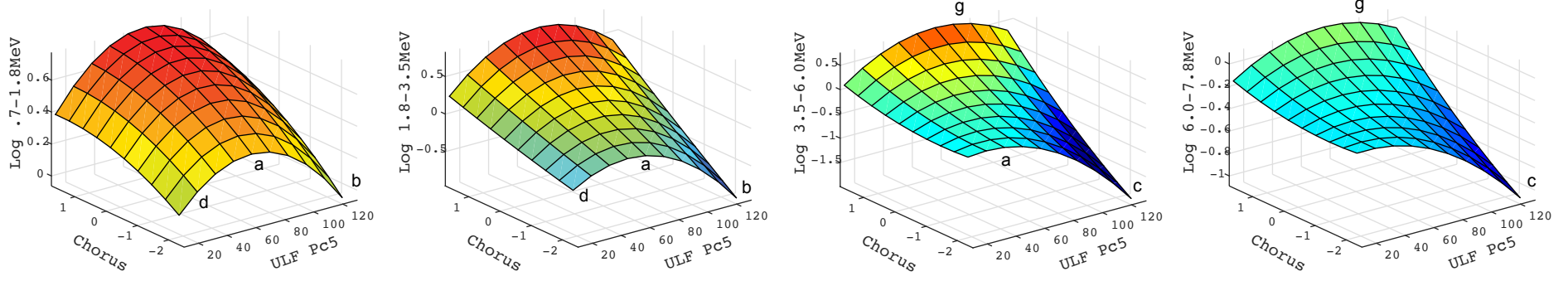
619

620

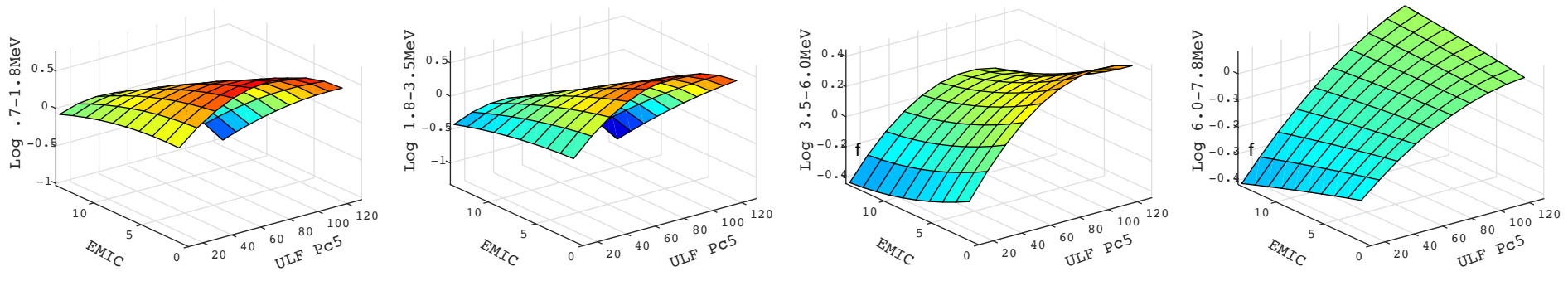
Figure 1.



A. ULF Pc5 X VLF Chorus



B. ULF Pc5 X EMIC



C. EMIC X VLF Chorus

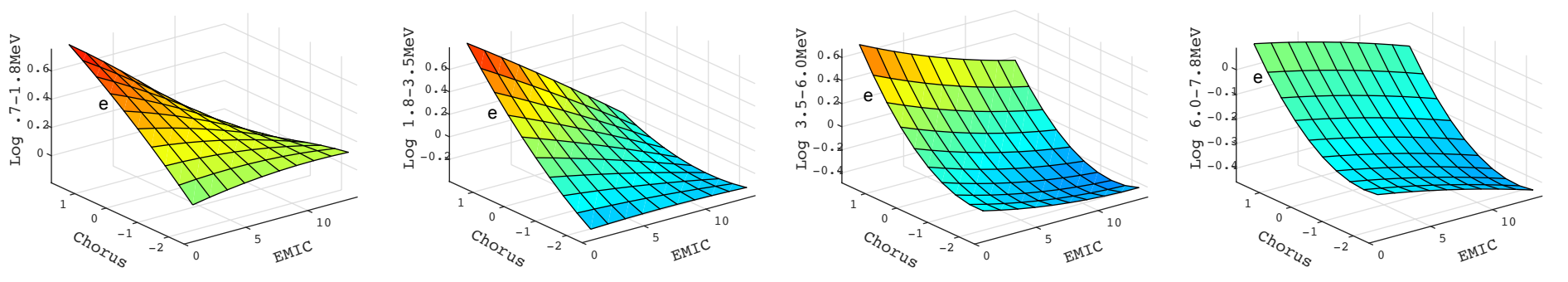
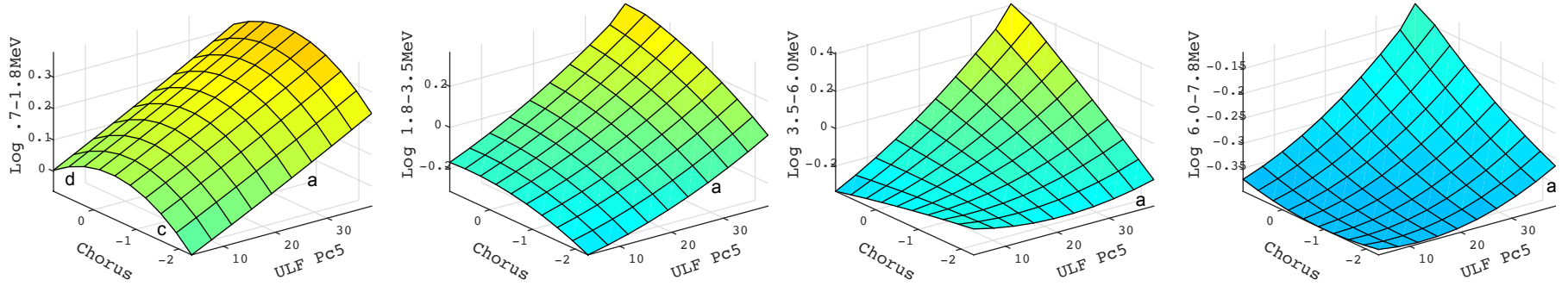


Figure 2.

ULF Pc5 X VLF Chorus



A. Kp < 2.3 (Lowest 3 quartiles)



B. Kp > 2.3 (highest quartile)

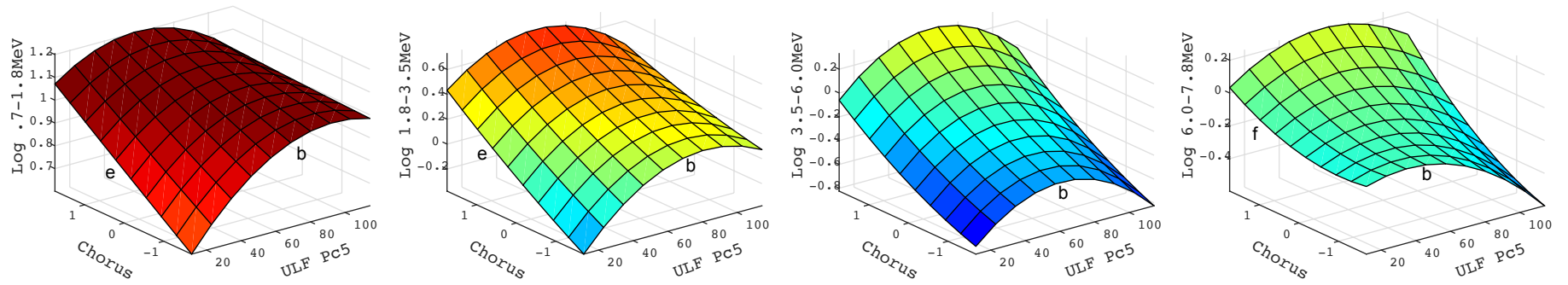
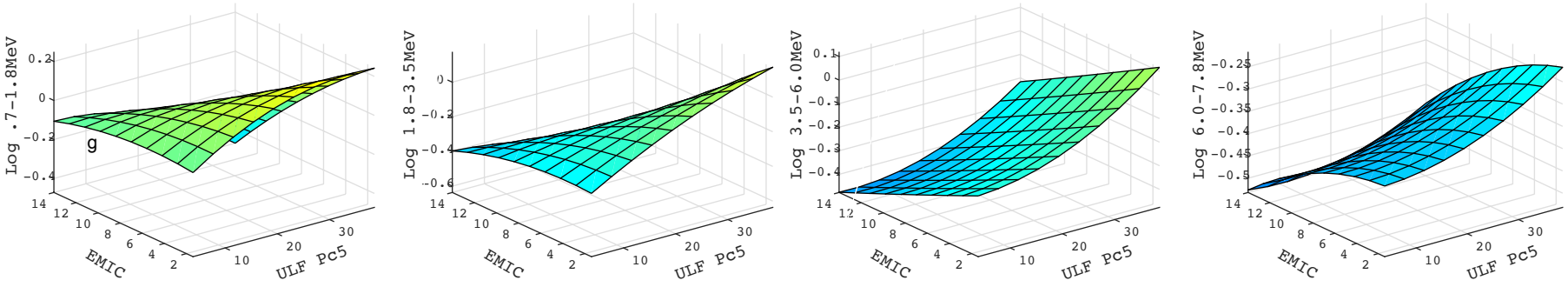


Figure 3.

ULF Pc5 X EMIC



A. Kp < 2.3 (Lowest 3 quartiles)



B. Kp > 2.3 (highest quartile)

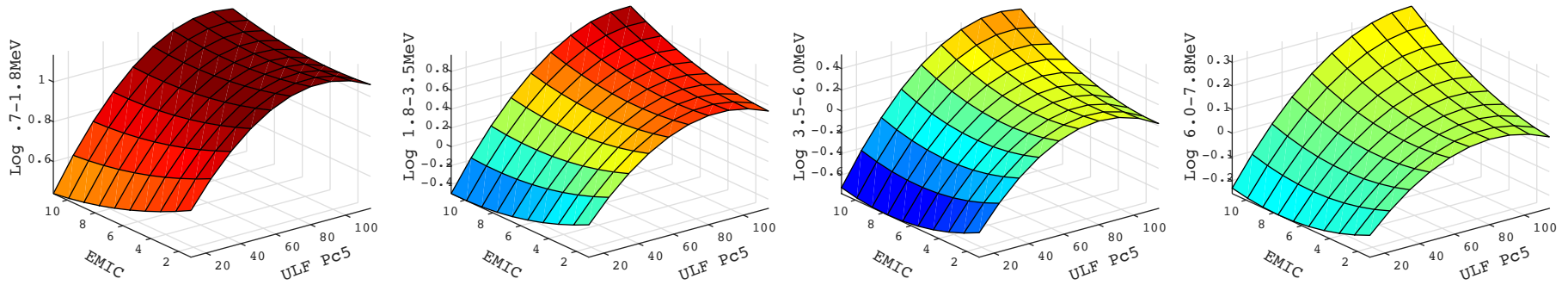
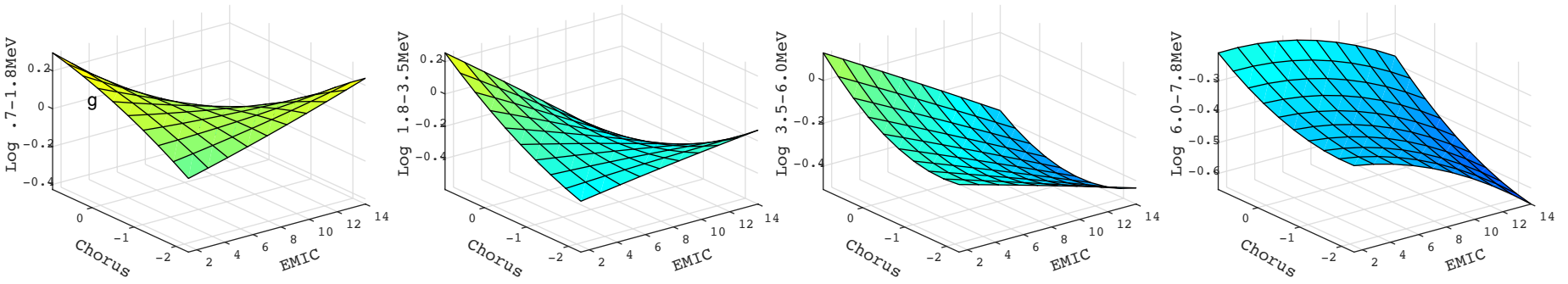


Figure 4.

EMIC X VLF Chorus

A. $K_p < 2.3$ (Lowest 3 quartiles)

Log electron flux
log electrons/(cm²/s/sr keV)



B. $K_p > 2.3$ (highest quartile)

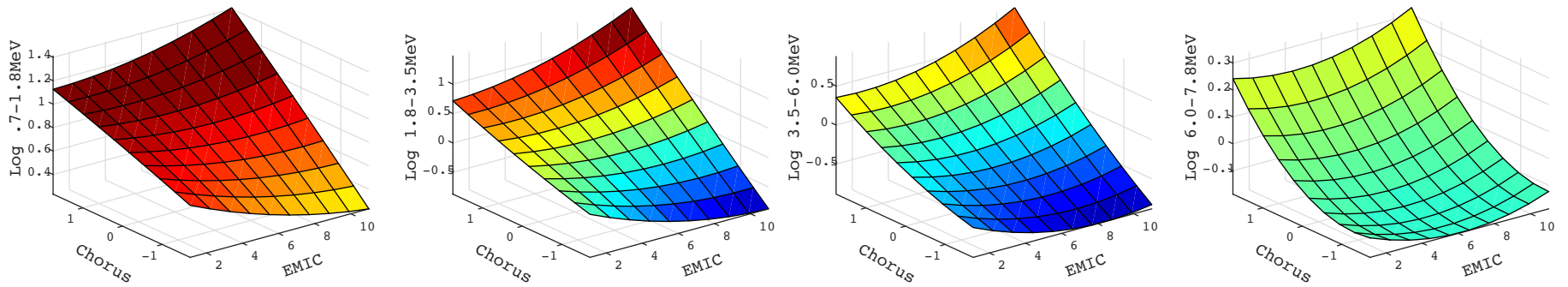
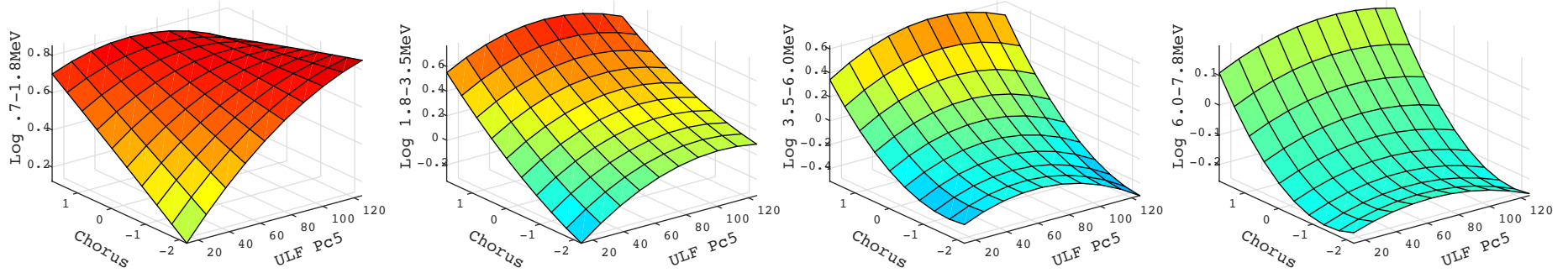


Figure 5.

ULF Pc5 X VLF Chorus



A. Southward: Avg Daily Bz < -0.3 (Lower third)



B. Northward: Avg Daily Bz > 0.5 (Upper third)

